Integration of a magnetocaloric heat pump in a low-energy residential building

Johra, Hicham; Filonenko, Konstantin; Heiselberg, Per Kvols; Veje, Christian T.; Lei, Tian; Dall'Olio, Stefano; Engelbrecht, Kurt; Bahl, Christian

Published in:
Building Simulation

DOI (link to publication from Publisher):
10.1007/s12273-018-0428-x

Publication date:
2018

Document Version
Accepted author manuscript, peer reviewed version

This is a post-peer-review, pre-copyedit version of an article published in [Building Simulation]. The final authenticated version is available online at: https://doi.org/10.1007/s12273-018-0428-x

Integration of a magnetocaloric heat pump in a low-energy residential building

Hicham Johra [a, *], Konstantin Filonenko [b], Per Heiselberg [a], Christian Veje [b], Tian Lei [c], Stefano Dall'Olio [c], Kurt Engelbrecht [c], Christian Bahl [c],

[a] *Aalborg University, Division of Architectural Engineering, Department of Civil Engineering, Thomas Manns Vej 23, DK-9220 Aalborg Øst, Denmark*

[b] *University of Southern Denmark, Center for Energy Informatics, Campusvej 55, DK-5230 Odense M, Denmark*

[c] *Technical University of Denmark, Department of Energy Conversion and Storage, Frederiksborgvej 399, DK-4000 Roskilde, Denmark*

** Corresponding author. Tel.: +45 9940 7234. E-mail address: hj@civil.aau.dk (H. Johra).*

Acknowledgements

This work was financed by the ENOVHEAT project, which is funded by Innovation Fund Denmark (contract no 12-132673).

Abstract

The EnovHeat project aims at developing an innovative heat pump system based on the magnetocaloric effect and active magnetic regenerator technology to provide for the heating needs of a single family house in Denmark. Unlike vapor-compression devices, magnetocaloric heat pumps use the reversible magnetocaloric effect of a solid refrigerant to build a cooling / heating cycle. It has the potential for high coefficient of performance, more silent operation and efficient part-load control. After presenting the operation principles of the magnetocaloric device and the different models used in the current numerical study, this article demonstrates for the first time the possibility to utilize this novel heat pump in a building. This device can be integrated in a single hydronic loop including a ground source heat exchanger and a radiant under-floor heating system. At maximum capacity, this magnetocaloric heat pump can deliver 2600 W of heating power with an appreciable average seasonal system COP of 3.93. On variable part-load operation with a simple fluid flow controller, it can heat up an entire house with an average seasonal system COP of 1.84.

Keywords

Magnetocaloric heat pump, magnetic heating, active magnetic regenerator, innovative heating system.

1. Introduction

In many countries, heat pumps now represent a key component of the energy development strategies. Consequently, researchers and industry strive to bring new cost-effective technical solutions to market. Conventional heat pumps and air-conditioner units are based on vapor compression technologies. They transfer thermal energy from a low-temperature to a high-temperature environment by means of irreversible thermodynamic cycles. In recent years, several research groups investigated the potential of the magnetocaloric effect for ambient temperature cooling applications. This innovative technology uses magnetocaloric materials (MCM) as solid refrigerants in magnetic cooling / heating cycle. Because of the reversible nature of the magnetocaloric effect, magnetic heating / cooling devices have a potential for high coefficient of performance (COP). In addition, they could also present the advantage of a more silent operation, efficient part-load control, a lack of toxic or greenhouse contributing gases, and the possibility for recycling the MCM and magnets at end-of-life (Smith et al. 2012). However, it has yet to prove its competitiveness compared to mature vapor compressor technologies (Eriksen et al. 2016).

The history of the active magnetocaloric regenerator cooling system started in 1982 with the proposal by Barclay of the active magnetic regenerator (AMR) cycle which is the basis for magnetocaloric heat pump (MCHP) systems (Barclay 1982). In 1998, an AMR device using superconducting magnets reached COPs above 6 (Zimm et al. 1998). Since then, different research groups have reported the performances of their AMR prototypes using permanent magnets for near-room temperature cooling. In 2012, Engelbrecht et al. presented a rotary AMR device operating with a maximum cooling capacity of 1010 W and a no-load temperature span of 25.4 K (Engelbrecht et al. 2012). In 2013, a Japanese group presented a device operating at a temperature

span of 5 K with a COP of 2.5 (Okamura and Hirano 2013). In 2014, Jacobs et al. reported the performances of a prototype achieving a zero temperature span cooling power of 3042 W and cooling power of 2502 W at a temperature span of 12 K with a COP above 2 (Jacobs et al. 2014). In 2016, a research team from the Technical University of Denmark published the study of a novel AMR device capable of 81.5 W of cooling power at a temperature span of 15.5 K and with a COP of 3.6 (Eriksen et al. 2016).

Some key topics are being investigated to improve the performance of magnetocaloric devices: development of new magnetocaloric materials, optimization of permanent magnet configurations, different regenerator geometries for efficient heat transfer and minimum pressure losses, novel designs for optimum operation and reduced parasitic losses of the whole machine (Eriksen et al. 2016; Lozano et al. 2016; Lei et al. 2017).

The "EnovHeat" project aims to tackle the aforementioned questions and develop the prototype of an innovative magnetocaloric heat pump (see Figure 1) able to provide for the heating needs of a single family house in Denmark (excluding domestic hot water production) with a higher COP than conventional systems (Bahl 2015).

Figure 1.

This article firstly introduces the operation principles of this novel MCHP and presents the numerical models of this device and the building case study used in this project. For the first time, the integration of this innovative heat pump as heating system in a building is discussed. The results of this numerical study are presented and the operation performance of the MCHP in a low-energy house is assessed. Finally, suggestions for further research on efficient control of this device are made.

2. Magnetocaloric heat pump

2.1. Operation of the magnetocaloric heat pump

A magnetocaloric heat pump transforms a low-quality thermal energy supplied by a low-temperature heat source into a high-quality thermal energy utilized by a high-temperature heat sink. This heat transfer is performed by means of a magnetic cooling / heating cycle, also known as the active magnetic regenerator (AMR) cycle. The refrigerant here is a solid material which exhibits a thermal response when the applied magnetic field changes. The magnetization (applying a magnetic field) of the refrigerant material induces an increase of its temperature and a decrease of its entropy. Reciprocally, the demagnetization (removing a magnetic field) of the refrigerant material leads to a decrease of its temperature and an increase of its entropy. This phenomenon is often reversible and is named the "magnetocaloric effect". Materials exhibiting this effect are called "magnetocaloric materials" and present a maximum magnetocaloric response at the ferro- to-paramagnetic phase transition called the "Curie temperature". The reference material for the magnetocaloric effect at room-temperature is Gadolinium. More information about the magnetocaloric effect and magnetocaloric materials can be found in Smith et al. 2012 and Kitanovski et al. 2015.

Figure 2.

The AMR cycle, at the core of the operation of this innovative heat pump, makes use of the magnetocaloric effect by alternatively magnetizing and demagnetizing a MCM with an external magnetic field source. The MCM solid refrigerant is contained as a porous media in a regenerator allowing bi-directional circulation of the coolant fluid transferring the thermal energy from the cold side to the warm side of the device. Figure 2 illustrates in details the AMR cycle. At the beginning of the cycle, there is a temperature gradient over the regenerator length and no magnetic field is applied: Figure 2(a). The cycle starts with an adiabatic magnetization of the MCM leading to a uniform temperature increase over the length of the regenerator: Figure 2(b). The heat transfer fluid is pushed from the cold side to the warm side of the AMR (cold-to-hot blow). The hotter fluid rejects the heat to the heat sink and the regenerator is cooled down at constant magnetic field: Figure 2(c). The magnetic field is removed and the regenerator operates an adiabatic demagnetization leading to a uniform temperature decrease over the length of the AMR: Figure 2(d). At the end of the cycle, the fluid is pushed back from the warm side to the cold side of the AMR (hot-to-cold blow) under zero-magnetic field, re-heating the bulk of the regenerator: Figure 2(e). Once the heat transfer fluid and the MCM reached local thermal equilibrium, the temperature distribution across the regenerator length is the same as at the initial state of the AMR cycle Figure 2(f). A detailed description of the AMR cycle can be found in the papers published by Lei et al. 2017 and Engelbrecht et al. 2012.

The MCHP prototype of the EnovHeat project is a rotary device with 13 packed bed spheres active magnetic regenerators placed on the stator and a two-pole permanent magnet assemblies placed on the rotor (see Figure 1). The regenerators consist of trapezoidal shaped-cassettes (see Figure 3) filled with first order MCM having a spherical shape with an average diameter of 450 μm. The spheres are kept together by an epoxy layer and the total amount of MCM is around 2.8 kg. The rotor is mounted on a vertical axis connected to an electric motor, and supports the two-pole magnet composed of 28 permanent magnet elements each. The rotation of the magnet creates a variating magnetic field having a maximum value of 1.4 T in the air gap. The 13 regenerators are connected to 2 manifold collectors and 2 manifold distributors: one of each on the cold side and on the hot side respectively. 13 high pressure and 13 low pressure solenoid valves allow synchronized regulation of the fluid flow through each of the regenerators. The circulation of the heat transfer fluid is performed by a single centrifugal pump (GRUNDFOS Data Booklet 2013).

Figure 3.

2.2. Numerical modeling of the magnetocaloric heat pump

The core of the magnetocaloric heat pump modeling process is the original one-dimensional numerical model created by Engelbrecht (Engelbrecht 2008) and further developed by Lei (Lei et al. 2017). The temperature gradient in the radial direction and the internal heat losses inside the regenerator are neglected, which leads to two coupled partial differential equations describing the fluid temperature distribution in the AMR with regards of time:

$$\frac{\partial}{\partial x}\left(k_{\text{disp}}A_c\frac{\partial T_f}{\partial x}\right)-\dot{m}_f c_f\frac{\partial T_f}{\partial x}-\frac{Nuk_f}{d_h}a_s A_c\left(T_f-T_s\right)+\left|\frac{\partial P}{\partial x}\frac{\dot{m}_f}{\rho_f}\right|=A_c\varepsilon\rho_f c_f\frac{\partial T_f}{\partial t} \quad (1)$$

$$\frac{\partial}{\partial x}\left(k_{\text{stat}}A_c\frac{\partial T_s}{\partial x}\right)+\frac{\text{Nu}k_f}{d_h}a_s A_c\left(T_f-T_s\right)=A_c\left(1-\varepsilon\right)\rho_s\times\left[c_H\frac{\partial T_s}{\partial t}+T_s\left(\frac{\partial s_s}{\partial H}\right)_{T_s}\frac{\partial H}{\partial t}\right] \quad (2)$$

Where *k*, *T*, ρ, *c* and *s* are the thermal conductivity, temperature, density, specific heat, and specific entropy; A_c, d_h, a_s, ε, *x*, *t*, $\dot{m}_f$, and *H* are the cross sectional area, hydraulic diameter, specific surface area, porosity of the regenerator bed, axial position, time, fluid mass flow rate and internal magnetic field; $\partial P/\partial x$ and *Nu* are the pressure drop and the Nusselt number. The subscripts *f* and *s* represent fluid and solid refrigerant, respectively. k_{disp} is the thermal conductivity of the fluid due to axial dispersion, k_{stat} is the static thermal conductivity of regenerator and fluid, and c_H is the specific heat capacity of the MCM at constant magnetic field. These equations are solved using implicit finite volume method implemented in MATLAB calculation programming software. This numerical model has been tested against experimental data and showed very good capabilities to predict the performances of real MCHP prototypes (Lei et al. 2017). However, this model is too computationally demanding to be used as is in building simulations. Because of the relatively fast operation of the MCHP, the numerical model outputs can be approximated by a series of quasi-steady states suitable for building simulations with time step size of 60 seconds. Therefore, the detailed MCHP model is run with the parameters of the EnovHeat prototype in order to generate around 1600 output points for building a set of 5-dimensional lookup tables. These lookup tables are implemented in MATLAB-Simulink function blocks and provide output fluid temperatures, heating and cooling powers, COP, magnetic work and fluid pressure losses as functions of the inlet fluid temperatures, operation frequency and fluid mass flow rate to the heat pump for very little computation time.

The additional elements of the MCHP are modeled in a simple way. The average electrical power usage of the set of valves (W_{valves}) has been measured directly on the prototype and has been found to be 63 W. The electrical power usage of the device's motor (W_{motor}) is calculated from the magnetic work of the AMR with the assumption of a motor efficiency factor equal to 0.65. Finally, the pump work (W_{pump}) is calculated with a polynomial function fitting the operation data provided by the manufacturer (GRUNDFOS Data Booklet 2013).

3. Building systems

The EnovHeat project aims at developing a novel heat pump system and demonstrating that it can provide for the heating needs of a low-energy single family house in Denmark. The following sections present the building case study chosen to test the integration of the MCHP, and the detailed dynamic building energy model developed for that purpose.

3.1. Building case study

A 150 m² single-story house with a typical geometry for dwellings in Denmark is chosen as case study (see Figure 4). With a yearly heating need of 16 kWh/m², the design fulfills the low-energy requirements of a new building "class 2020" of the Danish building regulation (Building Regulation 2010) and almost reaches the "Comfort House" standard (Larsen and Brunsgaard 2010). The main characteristics of the house case study can be found in Table 1.

Figure 4.

Table 1.

In the case of Danish dwellings, the most energy efficient configuration for heat pump systems is to couple a ground source heat exchanger (GSHE) with a hydronic radiant under-floor heating (UFH) (Den lille blå om Varmepumper 2011). The water-brine heat transfer fluid is chosen to be 20 volume% ethylene glycol and 80 volume% water.

Two types of GSHE are considered in this case study: a horizontal GSHE and a vertical borehole GSHE. The ground loops are designed according to international standards and manufacturer's guidelines (VDI 4640:2001; Uponor Ground Energy Technical Information 2012; Ground Source Heat Pump Project Analysis 2005) with the assumption that the soil is a humid clayey sand: thermal conductivity of 1.5 W/m.K; density of 1900 kg/m³; specific heat capacity of 1400 J/kg.K. The grouting material is chosen to be with a thermal conductivity of 1.4 W/m.K, a density of 1500 kg/m³ and a specific heat capacity of 1670 J/kg.K. Consequently, the horizontal GSHE is a 194 m long single collector with a serpentine layout. It is composed of PEX pipes with 40 mm outer diameter and 33 mm inner diameter. They are placed at a depth of 1.5 m with a pipe spacing of 1.5 m. The collector covers 291 m² of ground surface area. The vertical borehole GSHE is a single collector consisting of a double U-tube PEX pipe with outer diameter of 44 mm and inner diameter of 37 mm. The borehole has a depth of 100 m and a diameter of 160 mm. The spacing between the 2 U-tube legs is 80 mm. The total pipe collector length is 200 m.

The hydronic under-floor heating system is designed according to international standards and manufacturer's guidelines (EN 1264:2011; ISO 11855:2012; Uponor Heating and cooling solutions – Technical guidelines 2008). Each room has a 100 mm thick concrete screed with embedded PE-Xa pipes with outer diameter of 16 mm and inner diameter of 13 mm. They lay 60 mm below the surface of the concrete screed. The spacing between the pipe legs is 300 mm.

The outdoor conditions and solar gains are extracted from the national reference Danish weather file DRY 2013. The building is therefore assumed to be located in an open field around Copenhagen. It is considered that 4 persons are occupying the house according to a fixed weekly schedule. The equipment and people load schedules are based on typical Danish equipment use and people schedule for a residential house (Jensen et al. 2011). A detailed description of the building case study can be found in a DCE technical report (Johra and Heiselberg 2016).

3.2. Modeling of the building systems

A detailed multi-zone numerical model of the building case study is created with the MATLAB-Simulink software. Similarly to the HAM-tools (Kalagasidis et al. 2008), this model calculates heat transfer through building elements with a one-dimensional explicit finite volume method (FVM) formulation comprising a small number of control volumes. This formulation is also known as "Resistance-Capacitance" network (RC network). External walls, internal walls, ceilings and roof elements are subdivided into 5 thermal nodes for the 3 different material layers (external panel, insulation layer, internal panel). Floor elements are subdivided into 9 nodes for the 3 different material layers and the hydronic UFH system (underground layer, insulation layer, UFH concrete screed).

Inside each thermal zone, the inner surfaces and the indoor air temperature nodes are connected within a star network configuration with constant mixed convection/radiation surface thermal resistance coefficients. Thermal bridges, ventilation, air infiltration and windows heat losses are modeled using constant thermal resistances.

Direct and diffuse solar radiation and long-wave radiation to the sky are calculated for external surfaces as a function of the local weather conditions and the surface orientation. The internal loads and the indoor solar gains are distributed over the air nodes and the internal surfaces according to constant ratio factors. 70% of the internal gains are modeled as purely convective and the remaining 30% are distributed over all the indoor surfaces according to their surface area. Concerning the internal solar loads, 15% are modelled to go directly to the air node, 55% to go to the floor and 30% to go to the vertical walls of the thermal zone.

The hydronic UFH system and the horizontal GSHE are modeled similarly as horizontal heat exchangers embedded in a multilayer slab by coupling a "plug flow" model in a pipe with the ε-NTU method. The plug flow principle model accounts for the dynamics of the fluid pushed into the pipes when the flow rate is changing over time (TRNSYS 17 – Mathematical Reference). The ε-NTU method collapses the three-dimensional domain of a horizontal heat exchanger into a one-dimensional Resistance-Capacitance star network. The effectiveness of the heat exchanger is calculated by taking into account the equivalent interaction thermal resistance in the layer of the slab where the hydronic pipes are laid (ISO 11855:2012; Scarpa et al. 2009). The vertical borehole GSHE is simulated by coupling two plug flow pipe models in a triangular thermal RC network representing the complex thermal interaction between the U-pipe of the heat exchanger, the grout of the borehole and the surrounding soil domain (Diersch et al. 2011). The ground around the GSHE systems is simulated as a one-dimensional finite domain in a MATLAB state space function. Boundary conditions are defined by the weather condition and the undisturbed deep ground constant temperature. All the fluid properties of the brine, the convective heat transfer coefficient in the pipes and the pressure losses are calculated according to brine composition, fluid velocity, temperature and Reynolds number.

The 10 different thermal zones of the dwelling (9 rooms and an attic) are connected together in order to form the house case study multi-zone model. No direct air exchange between thermal zones

is considered. Because the heat equation is solved here with an explicit scheme, the simulation time step size is set constant to 60 seconds to avoid numerical instability.

The building numerical model has been validated with a BESTEST procedure. In addition, each sub-component of the building model has been validated against commercial software (COMSOL Multiphysics and BSim) or experimental test data. Validation test results and detailed description of the building model and its sub-components can be found in a DCE technical report (Johra and Heiselberg 2016).

4. Building systems

In order to achieve a high COP with heat pump systems, it is crucial to minimize the temperature span between the heat source and the heat sink. For that purpose, it is recommended to use ground source heat exchangers such as horizontal collectors or vertical boreholes in countries like Denmark. Although they have a significant investment cost, large amounts of thermal energy can be extracted from them at a higher and more stable temperature than outdoor air source systems, especially during the winter periods (Den lille blå om Varmepumper 2011). Concerning heat emitters, radiant under-floor heating systems offer a large surface of exchange with the indoor environment. They can therefore deliver an appreciable heating power with low inlet fluid temperature and keep the indoor air temperature lower than with radiator systems for an equivalent thermal comfort (Le Dréau 2014). As mentioned before, the magnetocaloric effect of a MCM is maximum around its Curie temperature. For some of these materials, the Curie temperature can be finely adjusted to match the temperatures inside the regenerator (Basso et al. 2015), taking into account its inherent temperature gradient (graded regenerator) (Smith et al. 2012). Consequently, the MCHP is designed for fixed optimum inlet and outlet temperatures which increases the importance of using a ground heat source which can provide a stable inlet fluid temperature.

Figure 5.

The principle of the AMR technology is to circulate the same fluid from one side of the system to the other. It is therefore possible to integrate the MCHP in a single hydronic loop without intermediate heat exchangers between the different sections of the circuit (see Figure 5). Because this heat pump can provide fluid flow rates and temperatures which are directly usable in a UFH system, a storage hot water tank is not needed. Such implementation has the potential of decreasing the effective temperature span between the heat source and the heat sink, but also simplifies the piping network and can therefore reduce the total installation costs and storage hot water tank heat losses. As mentioned before, the heat transfer fluid is circulated through the ground source loop, the UFH loops and the regenerators with only one circulation pump which can run at volume flow rates ranging from 100 L/h up to 2100 L/h with a net positive suction head ranging from 20 to 41 kPa (GRUNDFOS Data Booklet 2013).

The control of the MCHP in this case study is based on a simple volume flow rate regulation. Each of the 9 UFH hydronic loops of the house is equipped with a valve regulated by an ON/OFF controller connected to a room temperature sensor. If the room temperature is above the

temperature set point of 22 °C, the valve of the corresponding UFH loop is closed. If the room temperature drops below the temperature set point, the valve is fully open to provide a nominal fluid volume flow of 220 L/h. The speed of the circulation pump and the total heat pump flow rate are varied accordingly. If all the UFH loop valves are closed, the circulation pump and the MCHP are turned off.

In addition, this heat pump device can operate at different rotation frequencies from 0.5 Hz up to 2 Hz. This allows additional control capabilities for optimizing the COP in function of the fluid flow rate.

5. Results

All the results presented hereafter are calculated for a four-month heating period from the 1st of January to the 30th of April under Danish weather conditions (DRY 2013).

The COP is a common performance assessment index used for heat pump and refrigeration systems. Two different COPs are defined here to study the efficiency of the MCHP. The COP_{AMR} is calculated with the useful heating power $Q_{heating}$ delivered by the heat pump and only considering the work due to the AMR internal operation: regenerator hydraulic pressure losses $W_{pressureloss}$ and magnetic work $W_{magnetic}$. This calculation is similar to considering that the device is working with a perfect motor and a perfect pump. The COP_{system} is calculated with the heating power of the heat pump and considering all the work power which is necessary to operate the building heating system: circulation pump work W_{pump} ($W_{pressureloss}$ including the losses due to inefficiency), MCHP motor work W_{motor} ($W_{magnetic}$ including the losses due to inefficiency) and MCHP valves work W_{valves}. The heat losses through the heat distribution piping network of the house are not taking into account because they are included in the total heating output of the UFH system (Georges et al. 2017).

$$COP_{AMR} = \frac{Q_{heating}}{W_{pressureloss} + W_{magnetic}} \quad (3)$$

$$COP_{system} = \frac{Q_{heating}}{W_{pump} + W_{motor} + W_{valves}} \quad (4)$$

Initial tests are performed with the MCHP heating up only one thermal zone in the house case study: the living room. The total nominal flow of the heat pump is kept constant during the 4 months of the heating test period. The Figure 6 and Figure 7 present the results of 150 simulations where the average heating production, system power usage and seasonal COPs have been calculated for different total nominal heat pump fluid flows, 3 different AMR rotation frequencies and 2 kinds of ground loop heat source (horizontal GSHE and vertical borehole GSHE). It has to be noted that for low nominal volume flow rates, the heat pump does not provide enough heating power output and therefore runs continuously without being able to keep the set point temperature of 22 °C.

Figure 6.

Figure 7.

One can see on Figure 6 that the MCHP heating production and its power usage increase rather linearly with the total fluid flow. However, for the lowest operation frequency of 0.5 Hz, the performances of the MCHP drop for fluid mass flow rates above 1600 L/h. In addition, when the heat pump is connected to a horizontal GSHE, its heating capacity is significantly diminished because of the lower fluid inlet temperature provided by this ground loop heat source. One can notice that the major part of the MCHP power usage is due to the pump work. At maximum fluid flow rate of 2100 L/h, the system can deliver up to 2600 W of heating power with an average seasonal system COP of 3.93.

The Figure 7 illustrates the change of the average seasonal COP_{AMR} and COP_{system} in function of the total nominal mass flow rate. Concerning solely the AMR, its performance (COP_{AMR}) is maximum for low fluid flow rates and low operation frequency. However, even if the COP_{AMR} is significant, the heating power output is very limited at low flow rates while the energy usage of the circulation pump remains high. Therefore, the performance of the overall heating system (COP_{system}) is maximum at high fluid flow rates with operation frequency of 1 or 2 Hz. Here again, one can see that vertical borehole GSHE allows better MCHP performance compared to the horizontal GSHE. It should be noted that the temperature span between the cold and hot side of the AMR is increasing with the nominal flow rate from 12.3 °C to 19 °C for the vertical borehole GSHE and from 18 °C to 25.5 °C for the horizontal GSHE.

In a second case study, the MCHP is tested to heat the whole house. According to the aforementioned results, the operation frequency is kept constant at 1 Hz as it shows the best performance for the considered range of fluid flow rates. The Figure 8 presents the results of the four-month tests of heating up the house case study with the MCHP (the first test has a vertical borehole GSHE as heat source; the second test has a horizontal GSHE as heat source). One can see that the heating system always manages to keep the operative temperature of the house above the set point of 22 °C. The average temperature and maximum temperature inlet to the under-floor heating system are 25.42 °C and 28.50 °C respectively. The average temperature outlet of the vertical borehole GSHE is 8.17 °C (10% and 90% percentile of the temperature outlet are 6.89 °C and 9.30 °C respectively). The average temperature outlet of the horizontal GSHE is 2.42 °C (10% and 90% percentile of the temperature outlet are 0.93 °C and 4.51 °C respectively). One can see that the vertical borehole GSHE is a more stable heat source which can provide higher brine outlet temperature to the heat pump compared to the horizontal GSHE. The average temperature span between the heat source and the heat sink is 17.25 °C and 23.00 °C for the vertical borehole GSHE and the horizontal GSHE respectively.

Figure 8.

The Figure 9 shows the evolution of the COPs during the four month heating test period. All these results are daily running average. For the vertical borehole GSHE case, the seasonal average COP_{AMR} is 9.19 (10% and 90% percentile of the COP_{AMR} are 7.69 and 10.60 respectively) and the seasonal average COP_{system} is 1.84 (10% and 90% percentile of the COP_{system} are 0.84 and 2.96 respectively). For the horizontal GSHE case, the seasonal average COP_{AMR} is 6.39 (10% and 90% percentile of the COP_{AMR} are 5.31 and 7.48 respectively) and the seasonal average COP_{system} is 1.59 (10% and 90% percentile of the COP_{system} are 0.67 and 2.55 respectively). Once again, one can see that the higher heat source temperature provided by the vertical borehole GSHE allows better operation performances of the MCHP compared to the horizontal GSHE. However, it is noticeable that the total system COP is rather low compared to the results of the single room test. This is due to the fact that the MCHP does not often run at maximum fluid flow rate where the coefficient of performance of the device is greater.

Figure 9.

6. Conclusions

This article demonstrates for the first time the possibility to utilize a magnetocaloric heat pump for heating an entire building. This innovative heating device has been modeled as multi-dimensional lookup tables derived from a detailed numerical model in order to be tested with dynamic building energy simulations. It has been shown that it can be integrated in a single hydronic loop including a ground source heat exchanger and a radiant under-floor heating system. Such implementation does not require a storage hot water tank or additional circulation pumps or intermediate heat exchangers. At a constant maximum fluid flow rate of 2100 L/h, this magnetocaloric heat pump, when coupled to a vertical borehole heat source, can deliver up to 2600 W of heating power with an appreciable average seasonal system COP of 3.93. Moreover, the use of a vertical borehole as a heat source allows better performance of the heat pump because it can provide a more stable and higher fluid temperature inlet compared to a horizontal ground source heat exchanger.

However, when the magnetocaloric device is used to heat an entire house with several thermal zones regulated by simple ON/OFF controllers, the heating system often operates at part-load capacity which leads to low COPs. Therefore, the magnetocaloric heat pump average seasonal system COP implemented in a low-energy house under Danish weather conditions is 1.84 and 1.59 for a vertical borehole GSHE heat source and a horizontal GSHE heat source respectively.

Advanced control strategies used in demand side management for building energy flexibility such as indoor temperature set point modulation, could be an interesting solution to improve the operation performance of this magnetocaloric heat pump. This question will be addressed in further research.

References

Bahl CRH (2015). EnovHeat project summary: development of efficient novel magnetocaloric heat pumps. Available at http://www.enovheat.dk/Research/ProjectSummary. Accessed 30 Aug 2017.

Barclay JA (1982). Use of a ferrofluid as a heat exchange fluid in a magnetic refrigerator. *Journal of Applied Physics* 53, 4: 2887–2894.

Basso V, Küpferling M, Curcio C, Bennati C, Barzca A, Katter M, Bratko M, Lovell E, Turcaud J, Cohen L (2015). Specific heat and entropy change at the first order phase transition of La(Fe-Mn-Si)13-H compounds. *Journal of Applied Physics* 118.

Diersch HJG, Bauer D, Heidemann W, Rähaak W, Schätzl P (2011). Finite element modeling of borehole heat exchanger systems - Part 1. Fundamentals. *Computers and Geosciences*, 37: 1122–1135.

Engelbrecht K (2008). A Numerical Model of an Active Magnetic Regenerator Refrigerator with Experimental Validation. PhD Thesis, University of Wisconsin, Madison, Wisconsin, USA.

Engelbrecht K, Eriksen D, Bahl CRH, Bjørk R, Geyti J, Lozano JA, Nielsen KK, Saxild F, Smith A, Pryds N (2012). Experimental results for a novel rotary active magnetic regenerator. *International Journal of Refrigeration* 35, 6: 1498–1505.

Eriksen D, Engelbrecht K, Bahl CRH, Bjørk R (2016). Exploring the efficiency potential for an active magnetic regenerator. *Science and Technology for the Built Environment* 22, 5: 527–533.

European Committee for Standardization (2011). EN 1264:2011 - Water based surface embedded heating and cooling systems. Brussels, European Committee for Standardization.

Georges L, Iwanek T, Thalfeldt M (2017). Energy efficiency of hydronic space-heating distribution systems in super-insulated residential buildings. In: Proceedings of the 15th International Building Performance Simulation Association Conference and Exhibition (BS2017), San Francisco, USA, pp.1852–1861.

Grundfos Product Center (2013). GRUNDFOS Data Booklet - CR1-9 A-FGJA-E-HQQE 3x230/400 50Hz - Grundfos Pump 96478872. Available at http://product-selection.grundfos.com/product-detail.product-detail.html?lang=ENU&productnumber=96478872&productrange=gma&qcid=228594986. Accessed 30 Aug 2017.

International Organization for Standardization (2012). ISO 11855:2012 - Building environment design. Design, dimensioning, installation and control of embedded radiant heating and cooling systems. Geneva, International Organization for Standardization.

Jacobs S, Auringer J, Boeder A, Chell J, Komorowski L, Leonard J, Russek S, Zimm C (2014). The performance of a large-scale rotary magnetic refrigerator. *International Journal of Refrigeration* 37, 1: 84–91.

Jensen JB (Dansk Energi), Hvenegaard CM (Teknologisk Institut), Pedersen SV (Teknologisk Institut), Lindholm D (Dansk Energi) (2011). Den lille blå om Varmepumper (in Danish). Denmark, Dansk Energi.

Jensen RL, Nørgaard J, Daniels O, Justesen RO (2011). Person-og forbrugsprofiler: bygningsintegreret energiforsyning (DCE Technical Reports; Nr. 69). Denmark, Aalborg University: Department of Civil Engineering.

Johra H, Heiselberg P (2016). Description and Validation of a MATLAB-Simulink Single Family House Energy Model with Furniture and Phase Change Materials (DCE Technical Reports; No. 187). Denmark, Aalborg University: Department of Civil Engineering.

Kalagasidis AS, Rode C, Woloszyn M (2008). HAM-Tools, a whole building simulation tool in Annex 41. In: Proceedings of the IEA ECBCS Annex 41 Closing Seminar, Copenhagen, Denmark, pp. 21–35.

Kitanovski A, Tusek J, Tomc U, Plaznik U, Ozbolt M, Poredos A (2015). Magnetocaloric Energy Conversion: From Theory to Applications. New York: Springer International Publisher.

Larsen TS, Brunsgaard C (2010). Komfort Husene: erfaringer, viden og inspiration. Denmark, Saint-Gobain Isover a/s.

Le Dréau J (2014). Energy flow and thermal comfort in buildings - comparison of radiant and air-based heating and cooling system. Ph.D. thesis. Aalborg University: Department of Civil Engineering, Aalborg, Denmark.

Lei T, Engelbrecht K, Nielsen KK, Veje TC (2017). Study of the geometries of active magnetic regenerators for room temperature magnetocaloric refrigeration. *Applied Thermal Engineering*, 111: 1232–1243.

Lei T, Navickaite K, Engelbrecht K, Barcza A, Vieyra H, Nielsen KK, Bahl CRH (Submitted 2017). Passive characterization and active testing of epoxy bonded regenerators for room temperature magnetic refrigeration. *Applied Thermal Engineering*.

Lozano JA, Capovilla MS, Trevizoli PV, Engelbrecht K, Bahl CRH, Barbosa Jr JR (2016). Development of a novel rotary magnetic regenerator. *International Journal of Refrigeration*, 68: 187–197.

Okamura T, Hirano N (2013). Improvement of the performance of a room temperature magnetic refrigerator using Gd-alloy. *Journal of the Japan Society of Applied Electromagnetics and Mechanics* 21, 1: 10–4.

RETScreen International (2005). Ground-Source Heat Pump Project Analysis. Canada, Minister of Natural Resources Canada.

Scarpa M, Grau K, Olesen BW (2009). Development and validation of a versatile method for the calculation of heat transfer in water-based radiant systems. In: Proceedings of the 11th International Building Performance Simulation Association Conference and Exhibition (BS2009), Glasgow, USA, pp.27–30.

Smith A, Bahl CRH, Bjork R, Engelbrecht K, Nielsen KK, Pryds N (2012). Material challenges for high performance magnetocaloric refrigeration devices. *Advanced Energy Materials* 2, 11: 1288–1318.

The Danish Ministry of Economic, Business Affairs Enterprise, and Construction Authority (2010). Building Regulations. Available at http://bygningsreglementet.dk/file/155699/BR10_ENGLISH.pdf. Accessed 30 Aug 2017.

University of Wisconsin-Madison Solar Energy Laboratory, TRANSSOLAR Energietechnik GmbH, CSTB, TESS (2012). Type 31: Pipe Or Duct. In: TRNSYS 17 - Mathematical Reference. pp.186–188.

Uponor GmbH (2008). Heating and cooling solutions - Technical guidelines. Germany, Uponor GmbH.

Uponor GmbH (2012). Ground Energy Technical Information. Germany, Uponor GmbH.

Verlag des Vereins Deutscher Ingenieure (2001). VDI 4640:2001, Thermal use of the underground-Ground source heat pump systems. Germany, Verlag des Vereins Deutscher Ingenieure.

Zimm C, Jastrab A, Sternberg V, Pecharsky V, Gschneidner Jr K, Osborne M, Anderson I (1998). Description and performance of a near room temperature magnetic refrigerator. *Advances in Cryogenic Engineering*, 43: 1759–1766.

Tables

Table 1: Parameters of the building case study.

Figure Captions

Figure 1: CAD model of the magnetocaloric heat pump prototype of the EnovHeat project: “MagQueen”.

Figure 2: Active magnetic regenerator cycle consisting of four processes: (b) adiabatic magnetization; (c) cold-to-hot blow; (d) adiabatic demagnetization; (e) hot-to-cold blow.

Figure 3: CAD model of the regenerator for the magnetocaloric heat pump prototype.

Figure 4: Scheme of the house case study: a typical 150 m² single family house in Denmark.

Figure 5: Integration of a magnetocaloric heat pump in single hydronic loop with ground source and under-floor heating system.

Figure 6: Heating power production and power usage of the magnetocaloric heat pump as function of fluid volume flow.

Figure 7: COP of the magnetocaloric heat pump and the entire heating system as function of fluid volume flow.

Figure 8: Four-month test of heating up a house with a magnetocaloric heat pump.

Figure 9: Daily average COPs during the four-month heating test period.

Figure 1

Click here to download Figure figure 1.jpg

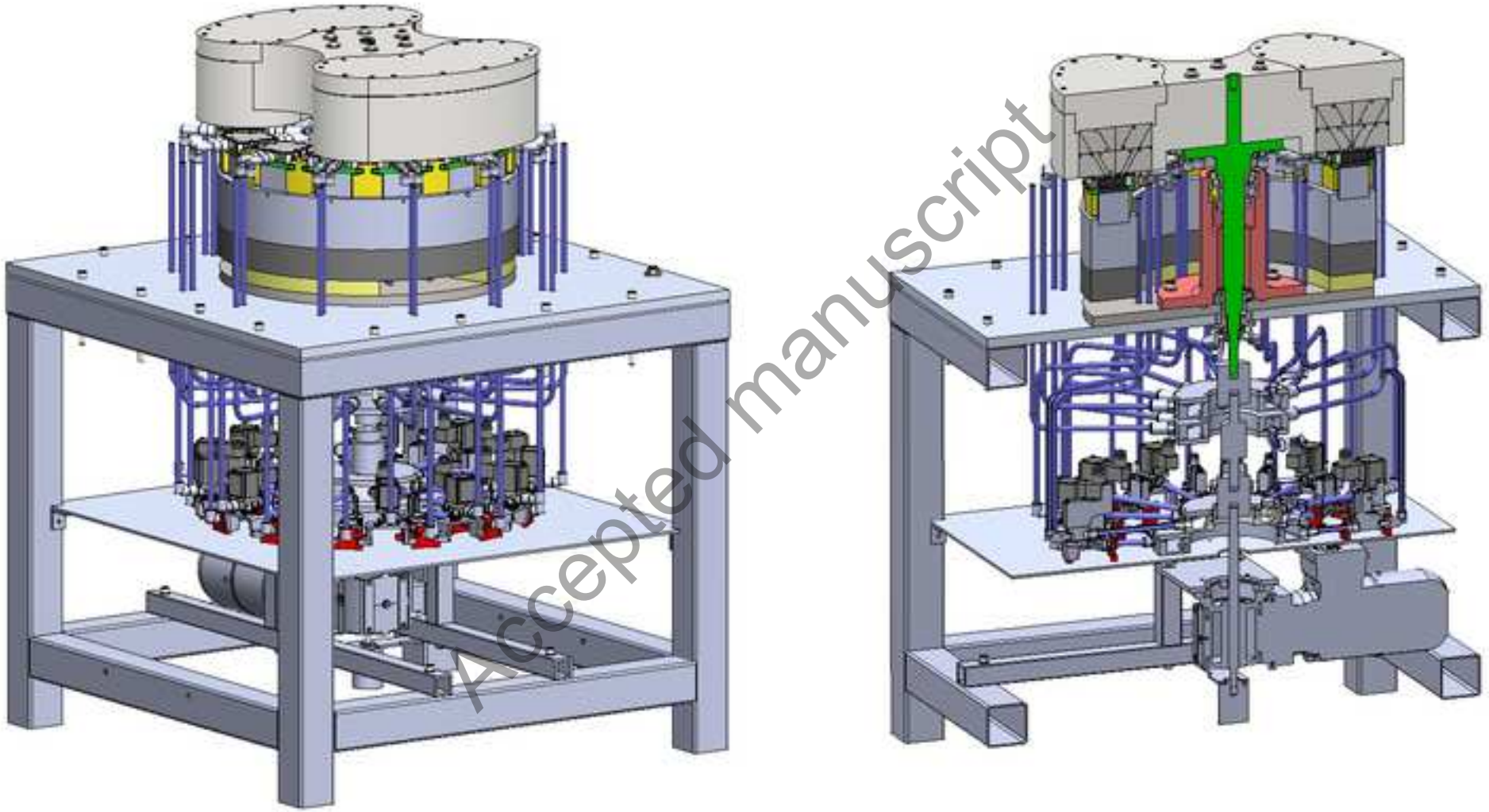

Figure 2

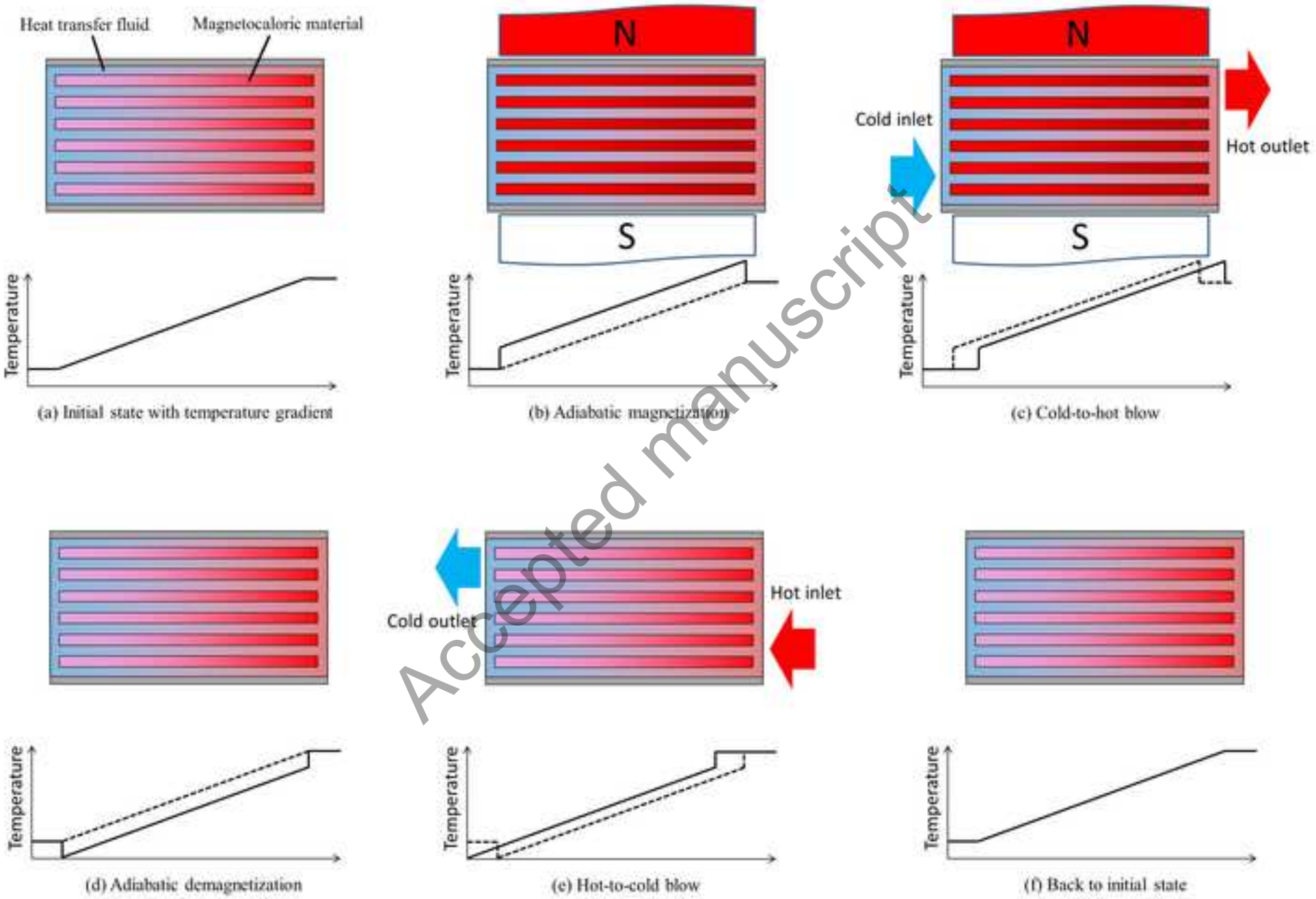

Figure 3

Click here to download Figure figure 3.jpg

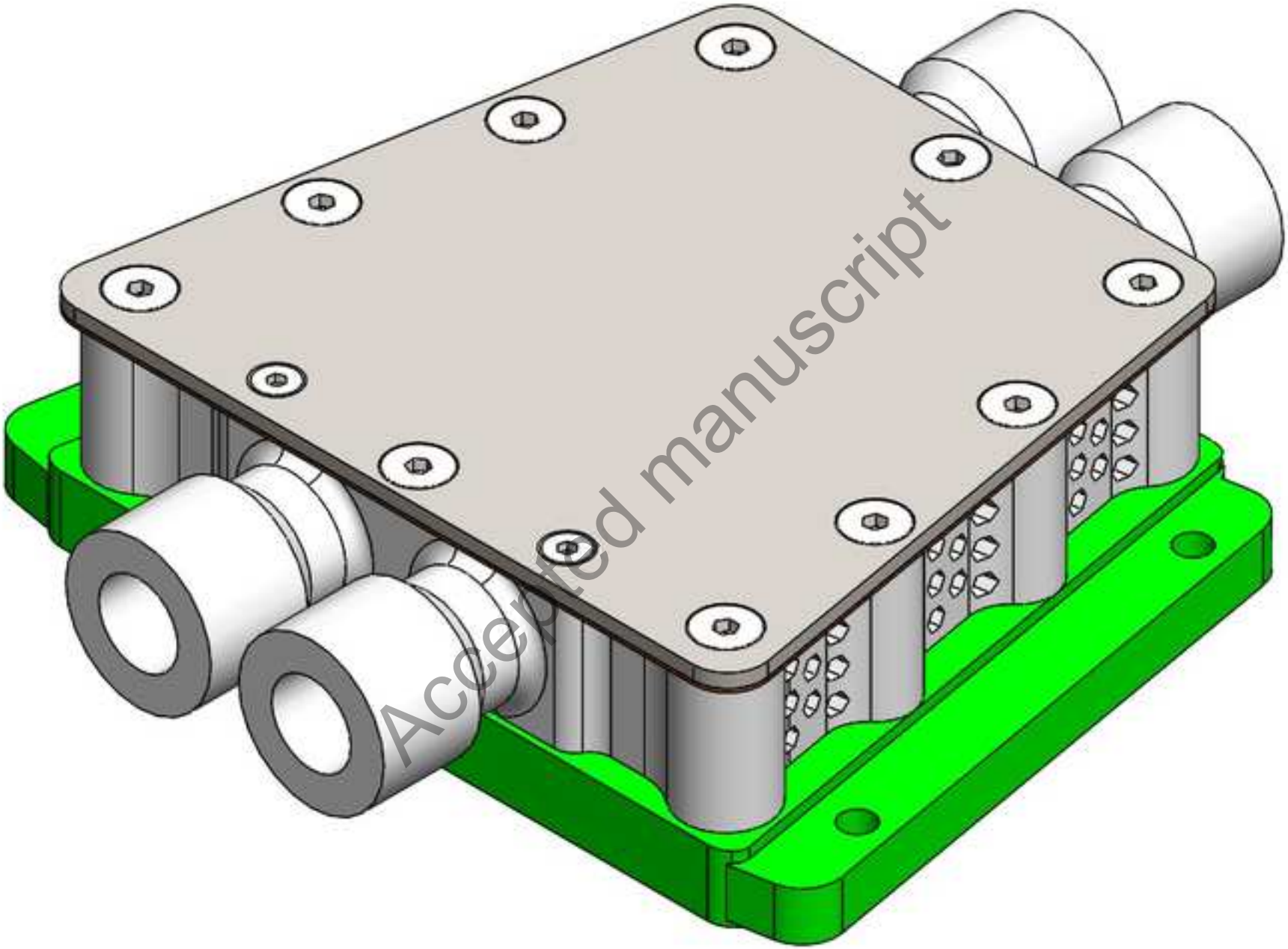

Figure 4

Click here to download Figure figure 4.jpg

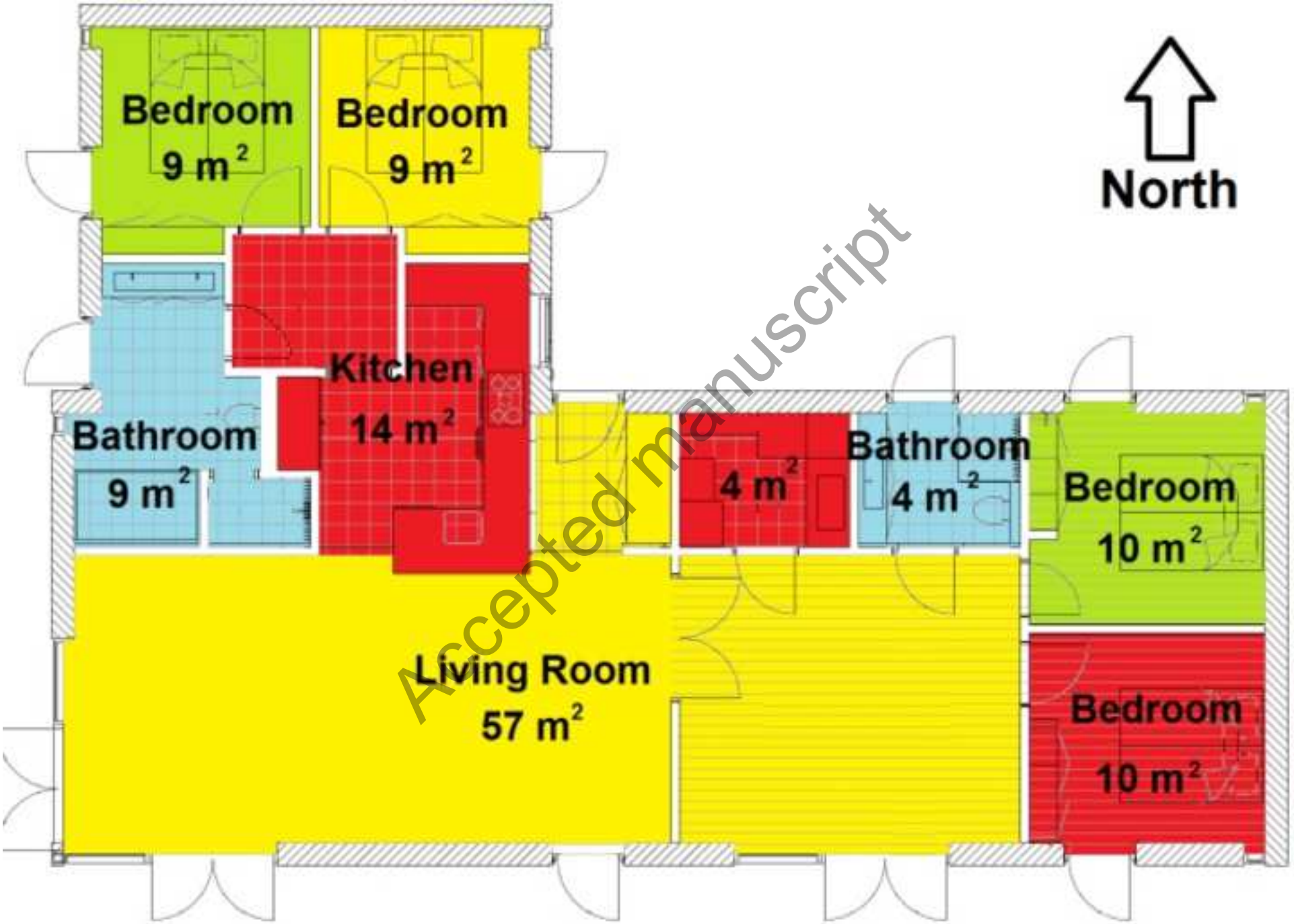

Figure 5

Click here to download Figure figure 5.jpg

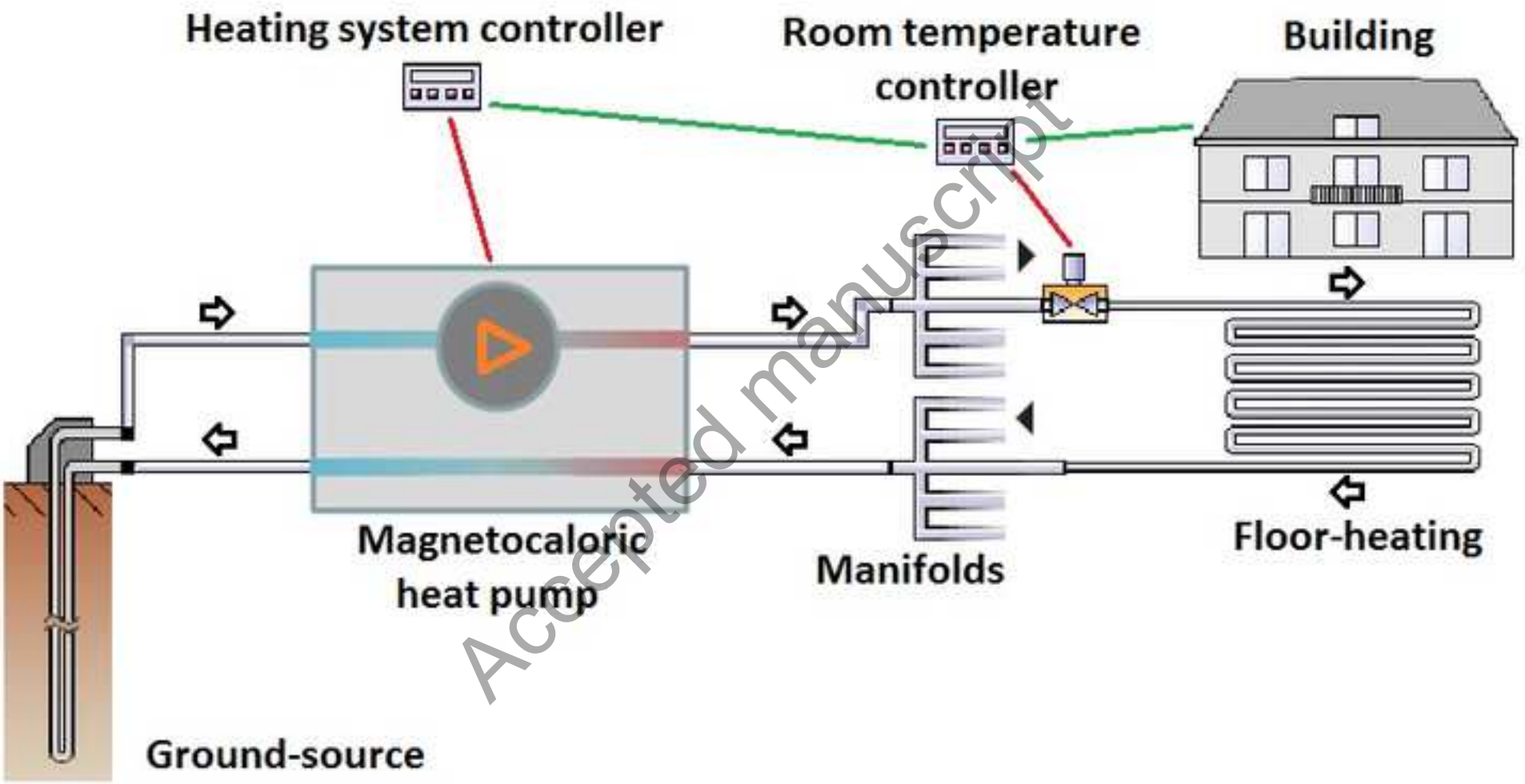

Figure 6

Click here to download Figure figure 6.jpg

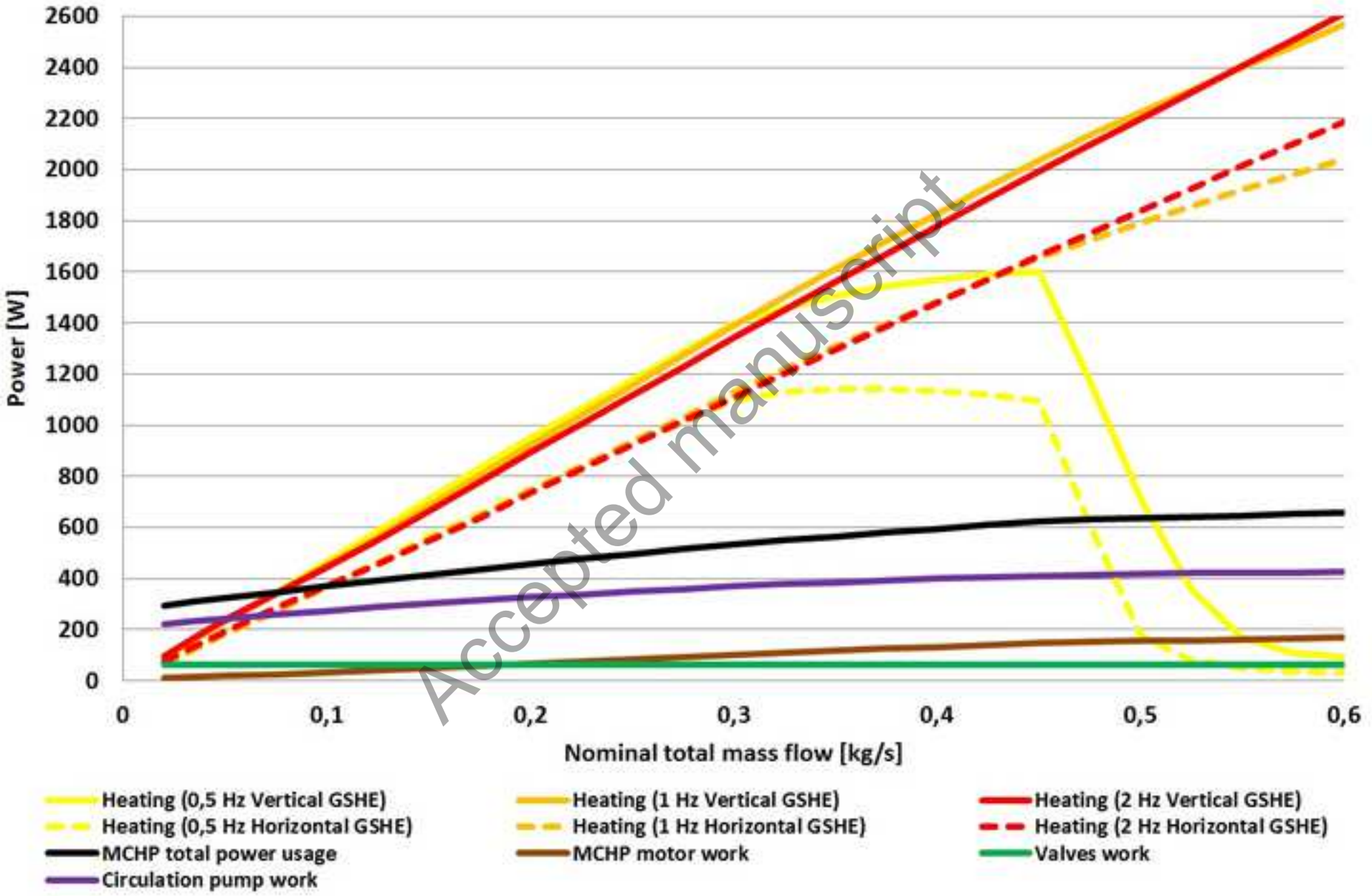

Figure 7

Click here to download Figure figure 7.jpg

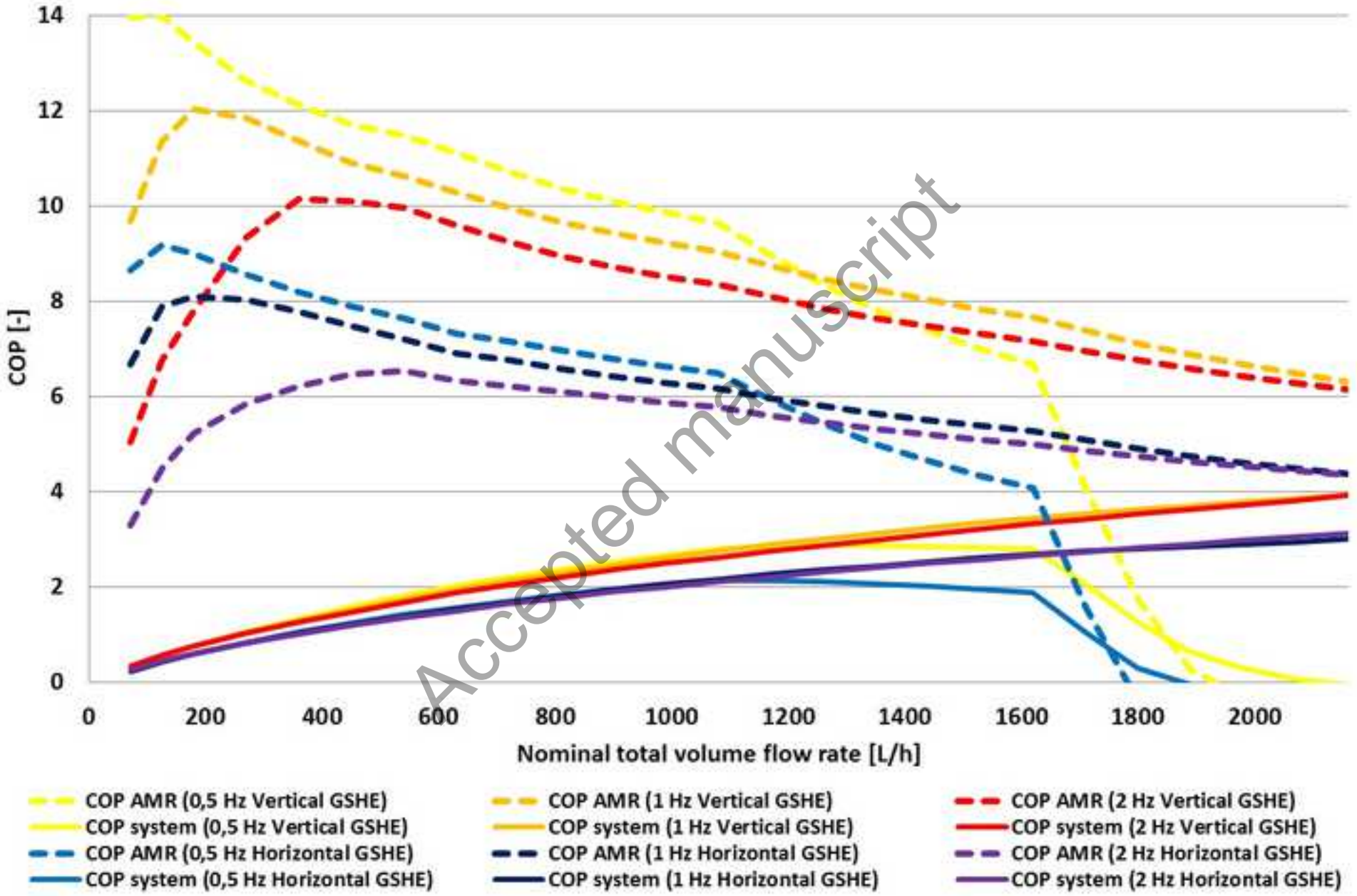

Figure 8

Click here to download Figure figure 8.jpg

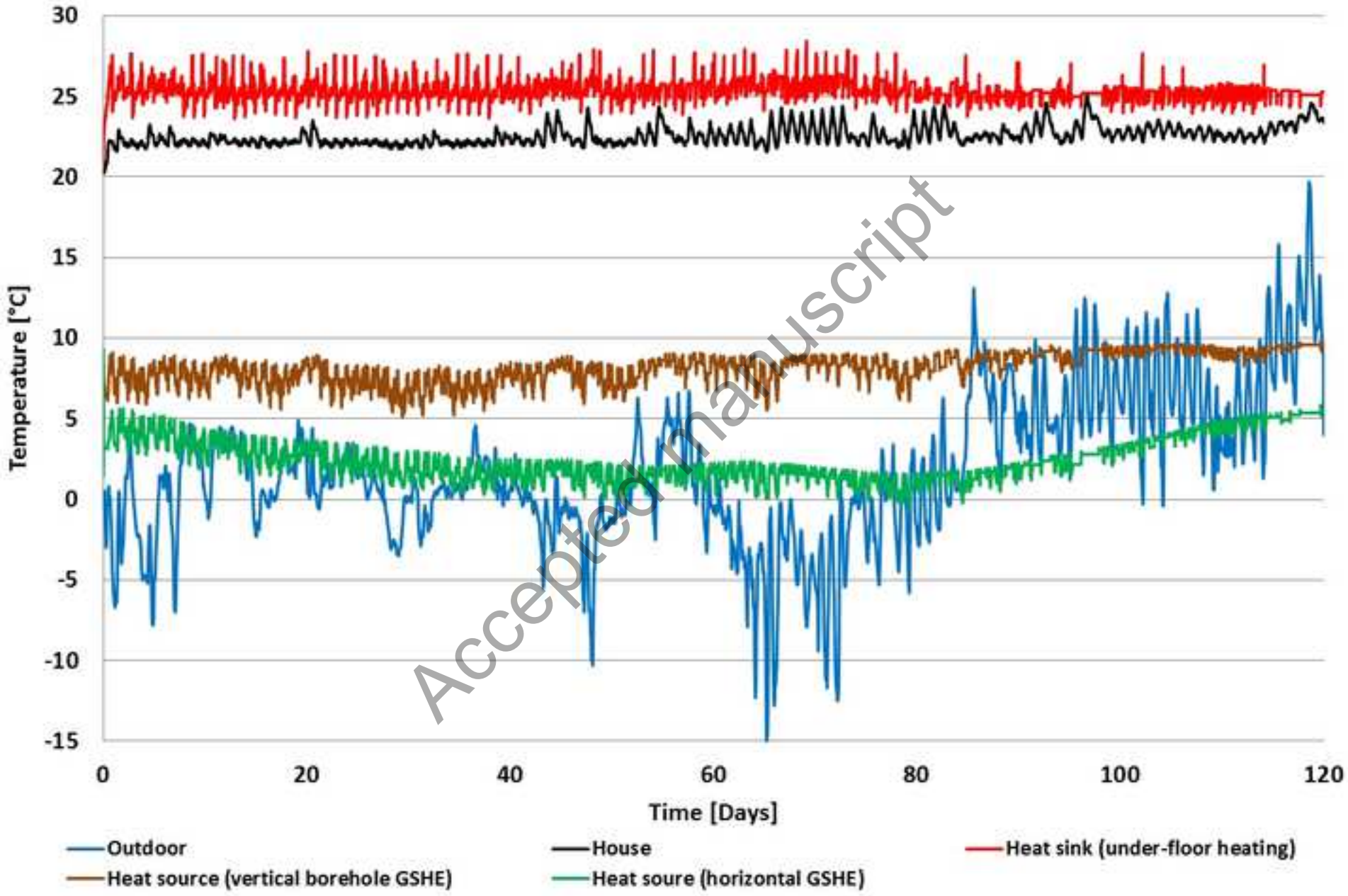

Figure 9

Click here to download Figure figure 9.jpg

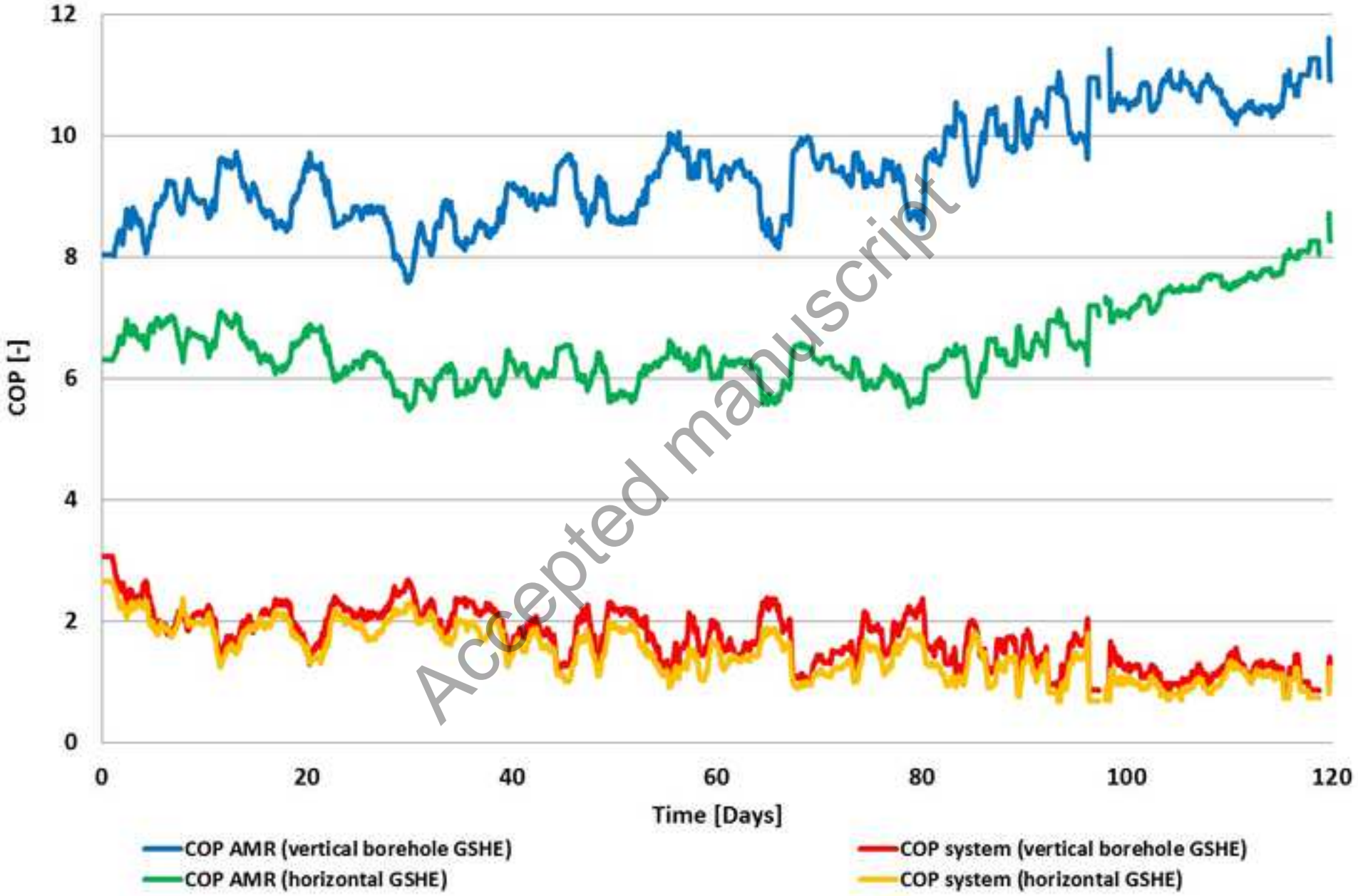

Table 1

Total ground floor area including walls [m²]	150
Heated floor area [m²]	126
Heated net volume [m³]	309
External walls U-value [W/m².K]	0.11
Floor U-value [W/m².K]	0.071
Roof U-value [W/m².K]	0.081
Doors and windows U-value [W/m².K]	1
Glazing transmittance [%]	0.63
Infiltration rate [h^{-1}]	0.1
Air change rate (without infiltration) [h^{-1}]	1.2
Ventilation heat recovery [%]	85
Heating temperature set point [°C]	22
Heating energy need (set point = 20 °C) [kWh/m². year]	16